Cohen, A. E., and P. Santos., 2012: South Florida flash flooding events. *Electronic J. Operational Meteor.*, **13** (11), 151–172.

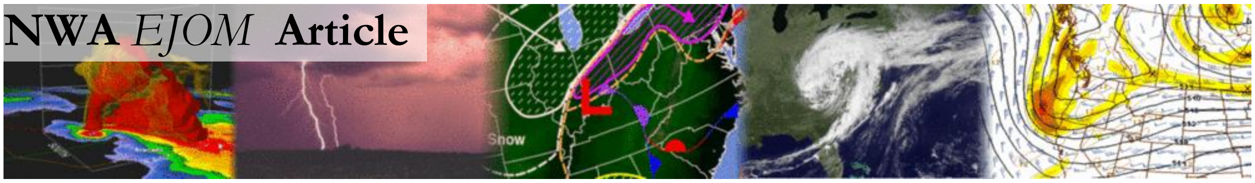

South Florida Flash Flooding Events

ARIEL E. COHEN
NOAA/National Weather Service/National Centers for Environmental Prediction/Storm Prediction Center, Norman, Oklahoma

PABLO SANTOS
NOAA/National Weather Service, Miami, Florida

(Manuscript received 17 August 2012; in final form 13 December 2012)

ABSTRACT

During the period from around 2200 UTC 30 October through 0800 UTC 31 October 2011, supercell thunderstorm activity produced excessive rainfall over parts of the Miami, Florida area, particularly affecting locations along the northwest and north coast of Biscayne Bay toward south Miami Beach. This event was partly responsible for setting a monthly record rainfall total at Miami Beach. What was unique about the thunderstorm activity was its long duration and nearly stationary motion. It also exhibited high precipitation efficiency, with rainfall rates in excess of 101.6 mm (4 in.) per hour. In this paper, we identify ways in which this relatively rare event may have been anticipated based upon available upper-air data, identification of heavy rainfall ingredients involved, consideration of supercell motion, and the use of very high resolution atmospheric models. The background synoptic environment is also addressed, which featured a surface front near the storm, and an onshore component of the low-level flow. Weather Research and Forecasting (WRF) model simulations are used to illustrate the role that mesoscale convergence zones may have played in exacerbating the event. Finally, two other similar cases are considered for purposes of comparison. This paper ultimately seeks to aid in the short-term anticipation of potential flash floods in association with non-tropical, deep-moist convection in south Florida.

1. Introduction

Non-tropical flash flood events across south Florida are relatively infrequent in the absence of stronger deep forcing for ascent more commonly found in higher latitudes and the presence of relatively flat terrain. However, the juxtaposition of rich, deep tropical or sub-tropical moisture and a conditionally unstable thermodynamic environment in the presence of weak low-level forcing for ascent does promote heavy rainfall (Doswell et al. 1996) on occasion over south Florida. This is especially the case during the summer, when diurnal sea breeze

Corresponding author address: Mr. Ariel E. Cohen, NOAA/National Weather Service, National Centers for Environmental Prediction, Storm Prediction Center, 120 David L. Boren Blvd., Norman, OK 73072
E-mail: Ariel.Cohen@noaa.gov

circulations offer low-level ascent (Burpee 1979). While more frequent during the summer, poleward excursions of moist, conditionally unstable environments do occur during the cool season, and can result in episodes of heavy rainfall (Strassberg 2009).

One such episode occurred from 2200 UTC 30 October through 0800 UTC 31 October 2011 over the Miami area. This event was responsible for more than 254 mm (10 in.) of rain that fell over coastal and metropolitan areas of far eastern Miami-Dade County surrounding Biscayne Bay affecting areas from Cutler Bay north-northeastward toward Coconut Grove and Coral Gables, and farther northeast toward downtown Miami and south Miami Beach. For simple geographical reference, these locations are highlighted in Figure 1. These precipitation values are derived from gauge-adjusted radar-derived quantitative precipitation estimates (Fig. 2). Much of this rain [i.e., over 152.4 mm (6 in.), in 6 hours] fell between 0000 UTC and 0600 UTC (Fig. 3), and a south Florida Water Management rain gauge in the Perrine area reported a rainfall rate of 107.7 mm (4.24 in.) per hour within the first half of this period.

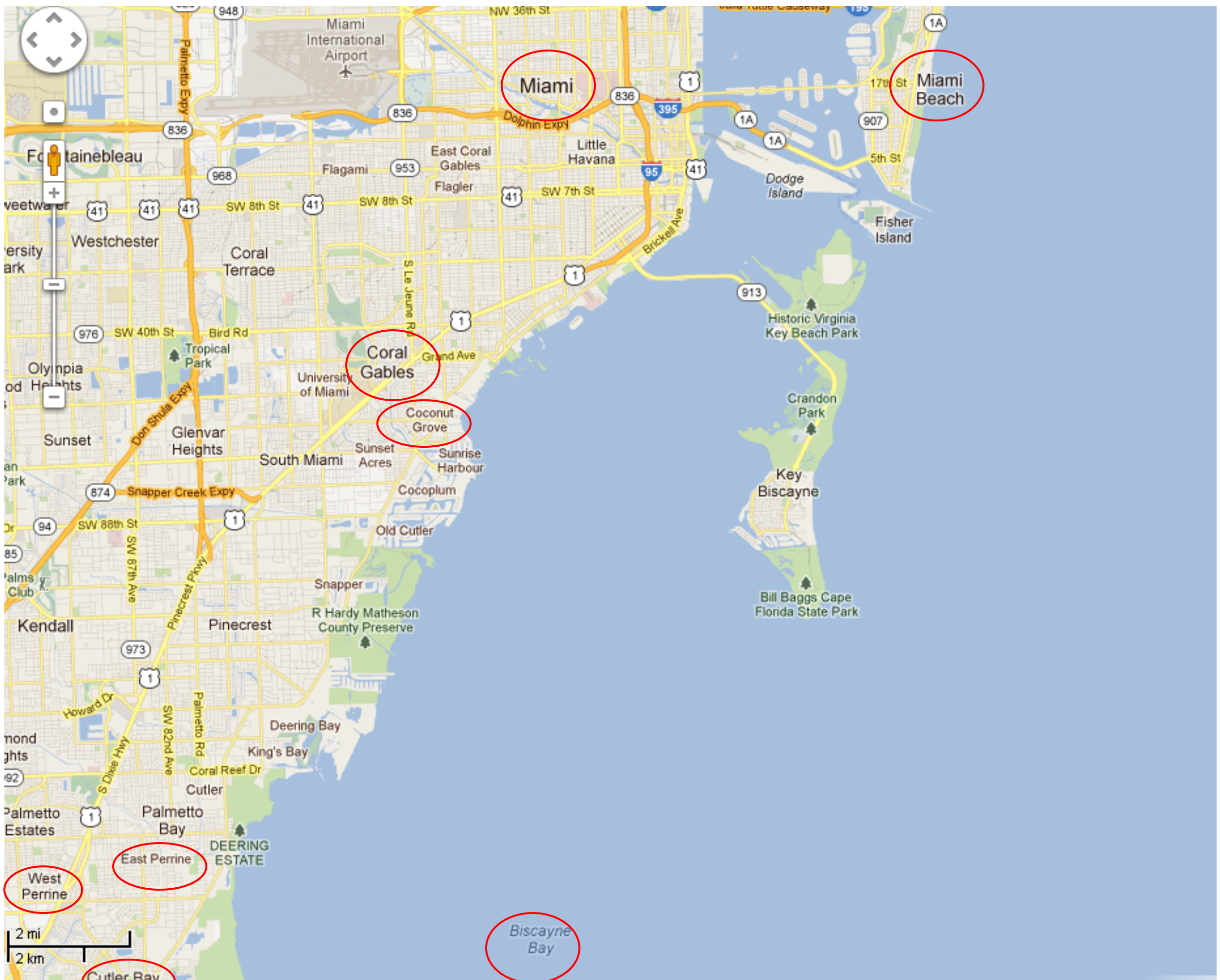

Figure 1. Map of Miami, Florida and its southeastern coastal communities (Google Maps 2012). Red ellipses have been placed around locations described within the introduction section.

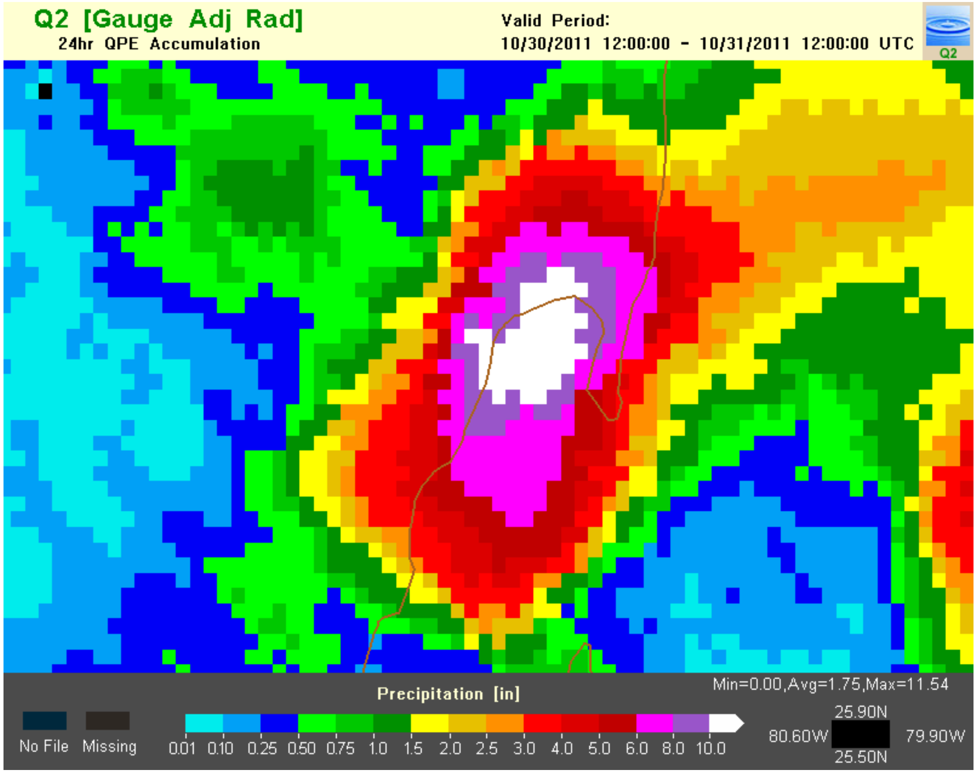

Figure 2. Gauge-adjusted, radar-derived precipitation amounts from 1200 UTC 30 October 2011 to 1200 UTC 31 October 2011.

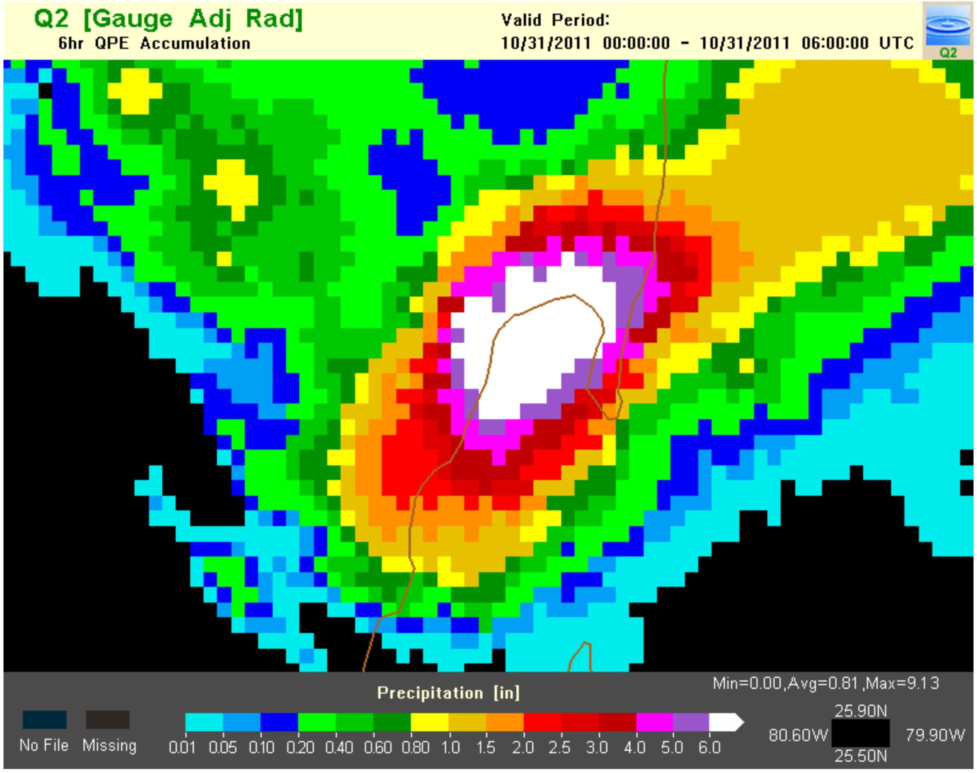

Figure 3. Gauge-adjusted, radar-derived precipitation amounts from 0000 UTC 31 October 2011 to 0600 UTC 31 October 2011.

Illustrating the rarity of this event, the Miami National Weather Service office issued a total of 12 Flash Flood Warnings during 2012, and four (one-third) of these warnings were directly related to this event. Each year from 2008 through 2010, no more than 8 Flash Flood Warnings were issued for precipitation unrelated to tropical cyclones. Forecasters' experience suggests that similar events occur roughly every two to three years. Examples from 2006 and 2009, exhibiting similarities to that from the 30-31 October 2011 case, will be presented in less detail toward the end of this study.

The convective mode involved in this excessive rainfall event was often characterized by a single, nearly stationary supercell thunderstorm featuring mostly weak and transient mid-level mesocyclones, with average rotational velocities predominantly below 30 knots. What was especially remarkable was the longevity of the nearly stationary storm, which was responsible for high-impact and severe flooding given its location relative to densely populated areas. The more than 304.8 mm (12 in.) of rain that fell over parts of the Miami metro area (e.g., Coconut Grove) caused flooding of numerous homes and substantial financial losses. As indicated by rainfall totals during the preceding couple of days displayed in Fig. 4, the situation was exacerbated by antecedent rainfall. For additional details on this flash flood event, please reference this summary of the event from the National Weather Service Weather Forecast Office in Miami, FL.

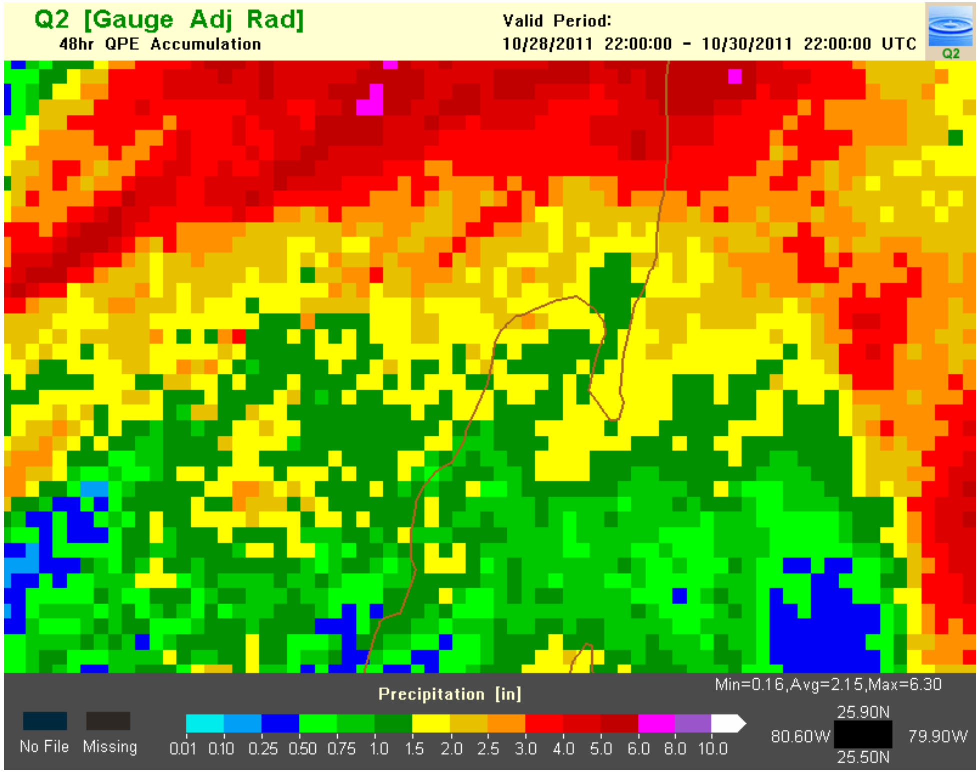

Figure 4. Gauge-adjusted, radar-derived precipitation amounts from 2200 UTC 28 October 2011 to 2200 UTC 30 October 2011.

Whether or not such an event can be forecast, and with how much skill, accuracy, and precision on both spatial and temporal scales are all of importance to forecasters. Clearly, such a forecast is of utmost importance given the event's adverse impact to both life and property.

However, do we have reasonable ability through observations and model output to make such a forecast with any consistent chance for positive verification? We attempt to address this crucial question via both observational data and high-resolution model output in the succeeding sections. Brief (given the scope of this paper) comparisons to other instances of flash-flood-producing convection across south Florida will also be presented.

2. Analysis of the 30-31 October 2011 flash flood event

The basic premise behind the ingredients of a flash flooding event are simple and are described by C. F. Chappell and cited by Doswell et al. (1996): "*the heaviest precipitation occurs where the rainfall rate is the highest for the longest time*." It follows that convection that exhibits nearly stationary motion would offer the largest duration of rainfall rates (e.g., Chappell 1986 and Doswell et al. 1996), maximized in areas where storm duration is longest. As addressed by Chappell (1986), the mean flow through a deep layer of the troposphere modulates the motion of convection. However, other processes, such as propagation (illustrated by Doswell 1996), and internal dynamics of a supercell storm (Bunkers et al. 2000) also modulate the motion and duration of convection. Ultimately, most precipitation systems that produce flash flooding are associated with slow motion of the systems (Chappell 1986), and some synoptic and mesoscale patterns have been identified that characterize systems featuring limited system motion (Maddox et al. 1979).

This particular case in Miami presented a unique challenge in identifying physical processes that limited storm motion. However, by no means was this high-impact event in Miami unique. Similar meteorological conditions existed between the environment that supported the Fort Collins, Colorado flash flood event of 28 July 1997 (Petersen et al. 1999) and the Miami event, especially with regard to the thermodynamic characteristics supporting heavy rainfall rates (addressed within the succeeding sections). Despite large differences in the land surface properties that exist between the two locations, the same basic principles of low-level circulations offering enhanced ascent (i.e., orographic versus coastal-related effects) to foster convective growth were present in both cases. Other high-impact cases of flash flooding sharing some characteristics with the Miami case have been addressed in Maddox et al. (1978), Maddox et al. (1979), and Caracena et al. (1979). A discussion of some of these ingredients follows.

a. Precipitation efficiency

The Miami, Florida 0000 UTC radiosonde observation (RAOB) sounding on 31 October (Fig. 5) illustrates many of the key ingredients supporting precipitation efficiency. A deep, nearly saturated layer existed from just above the surface through the lower and middle troposphere, with a lifting condensation level (LCL) height around 150 m above ground for a surface-based parcel. Negligible potential for sub-cloud evaporation existed beneath the LCL. Weak low- to mid-level lapse rates (i.e., 5.5°C km^{-1} in the 850-500-mb layer) yielded a "narrow" CAPE profile that prevented substantial vertical accelerations from occurring, and, in turn, increased the residence time for precipitation particles growing within the cloud [Note: the parcel trace plotted in this sounding incorporates the virtual temperature correction in its formulation (Doswell and Rasmussen 1994)]. Furthermore, given the deep layer of near-saturation below the relatively high melting level around 4.5 km above ground level (AGL), the warm-cloud layer

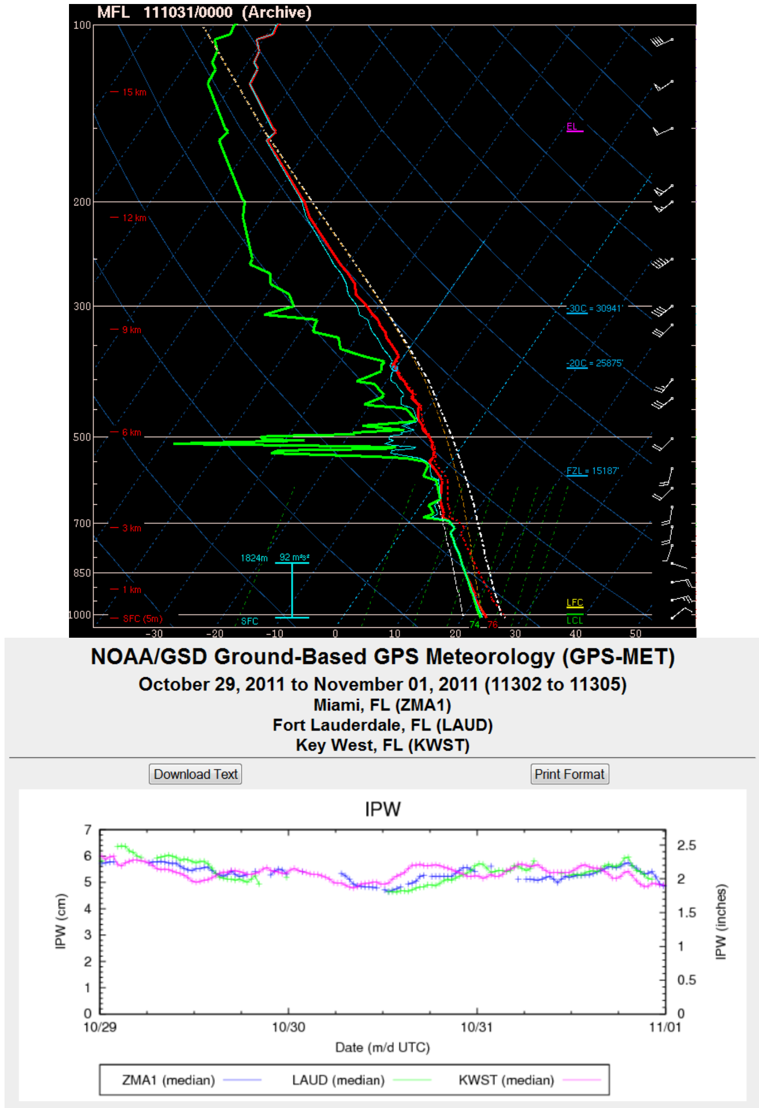

Figure 5. Top panel shows observed sounding data at 0000 UTC 31 October 2011 from Miami, FL. Solid red line depicts environmental temperatures, dashed red line depicts environmental temperature profile incorporating the virtual temperature correction (Doswell and Rasmussen 1994), green line depicts environmental dewpoints, thicker dashed white line depicts the parcel temperature trace for an ascending surface-based parcel incorporating the virtual temperature correction, dashed brown line depicts the parcel temperature trace for an ascending surface-based parcel without incorporating the virtual temperature correction, thinner dashed white line depicts the parcel temperature trace for a descending parcel. Output display is provided by National Centers Advanced Weather Interactive Processing System Skew T Hodograph Analysis and Research Program. Bottom panel shows similar estimates for a 3-day period around 0000 UTC 31 October 2011 from NOAA Global Systems Division (GSD) GPS Meteorology network for three sensors across South Florida including Fort Lauderdale, Miami, and Key Biscayne. These sensor estimates are based on microwave retrievals known to suffer of little precipitation bias (Gutman et al. 2004).

was deep. These factors supported warm rain and collision-coalescence processes yielding high precipitation efficiency. Many of these thermodynamic factors resembled those present during the Fort Collins case (Petersen et al. 1999).

b. Moisture content

Per the aforementioned Miami RAOB, rich low-level moisture, with a lowest 100-mb mean mixing ratio of 16.4 g kg^{-1}, coupled with abundant deep-layer tropospheric moisture content, also supported heavy rain. In fact, analysis of water vapor imagery from 0000 UTC 31 October 2011 reveals that this was the result of a moisture plume connection to the northwest Caribbean Sea (not shown). Highlighting the rich moisture, the measured sounding based precipitable water value was 56.6 mm (2.23 in.), which was around 2 standard deviations above the climatological mean for late October. This precipitable water value was also around the 99th percentile for precipitable water values for that time of the year (Bunkers 2006). The easterly component in the low levels likely aided in enhancing the influx of low-level moisture resulting from moisture fluxes atop the Gulf Stream. While the sounding indicates that this value may have been influenced by cloud condensate on the radiosonde, a similar precipitable water value of 55.4 (2.18 in.) at Key West at 0000 UTC 31 October, and numerical weather prediction model output, corroborate the Miami observation, illustrating the anomalous amount of moisture that was in place. Furthermore, similar values across the area were also observed by NOAA's Global Systems Division GPSMET network (Fig. 5).

c. Ascent

Forcing for ascent within the mid and upper levels was very modest, at best. South Florida was at the leading edge of a broad mid- and upper-level, high-amplitude trough, with an axis extending into the western Gulf of Mexico (Fig. 6 and Fig. 7). With only negligible mid-level height changes over the southeastern states observed over the preceding 12 hours, little, if any, differential cyclonic vorticity advection can be inferred in this scenario, though some weak contribution to large-scale ascent over south Florida may have occurred within the right-entrance region of an upper-level jet stream east of the trough (Fig. 6). Furthermore, only weak warm air advection appears to be present across south Florida (Fig. 8), contributing little toward ascent.

A tight, west-to-east oriented dewpoint gradient appears to have been draped across the central Florida peninsula evident at 850 mb (Fig. 8). This dewpoint gradient was likely also associated with a surface theta-e gradient situated across the southern Florida peninsula at 0300 UTC (Fig. 9). These charts collectively illustrate the northward-sloping frontal surface over the central and southern Florida peninsula. While convergence associated with spatial gradients in the wind direction at the surface appeared minimal in surface observations, the ascending branch of the frontal circulation on the warm/moist side of the surface boundary may have contributed to lifting parcels to their levels of free convection to support storm development. Furthermore, the trajectories of parcels from over-water to over-land likely established a coastal convergence zone related to the influence of inland friction whereby the reduction in the flow over inland areas relative to offshore areas results in horizontal wind speed variations favoring low-level convergence. This aspect will be explored in further detail using high-resolution modeling later in this paper.

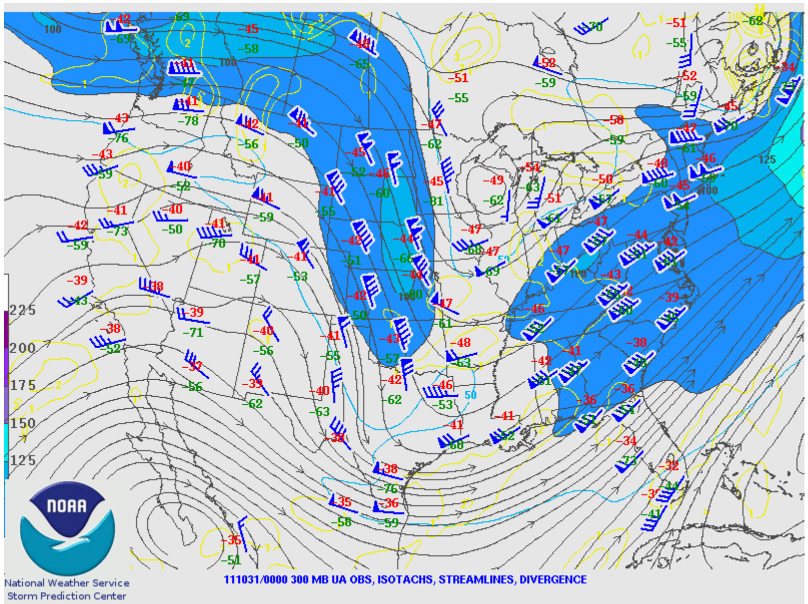

Figure 6. 300-mb observations and objectively-analyzed 300-mb streamlines (in black) and divergence (in yellow) for 0000 UTC 31 October 2011 including isotachs (in light blue color fill), and wind barbs (corresponding wind speeds in knots).

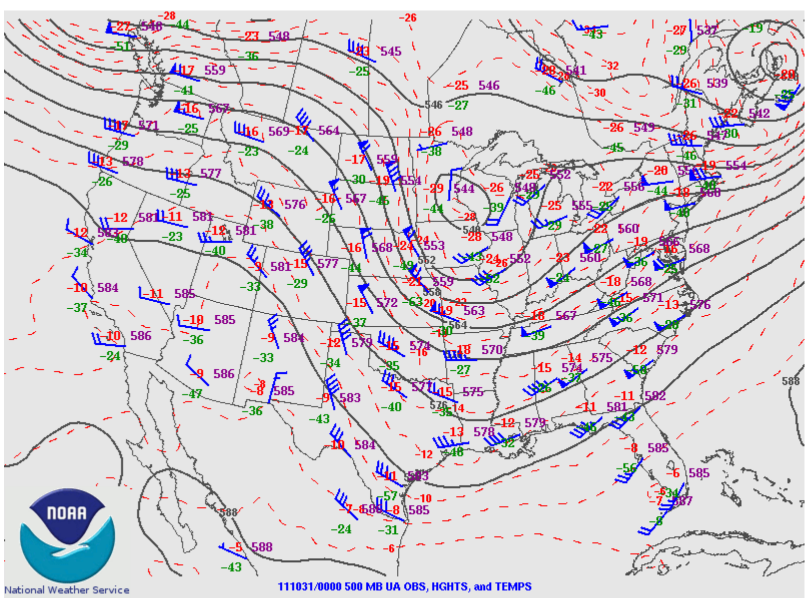

Figure 7. 500-mb observations and objectively-analyzed 500-mb heights (black), isotherms (dashed red), and wind barbs (corresponding wind speeds in knots) at 0000 UTC 31 October 2011.

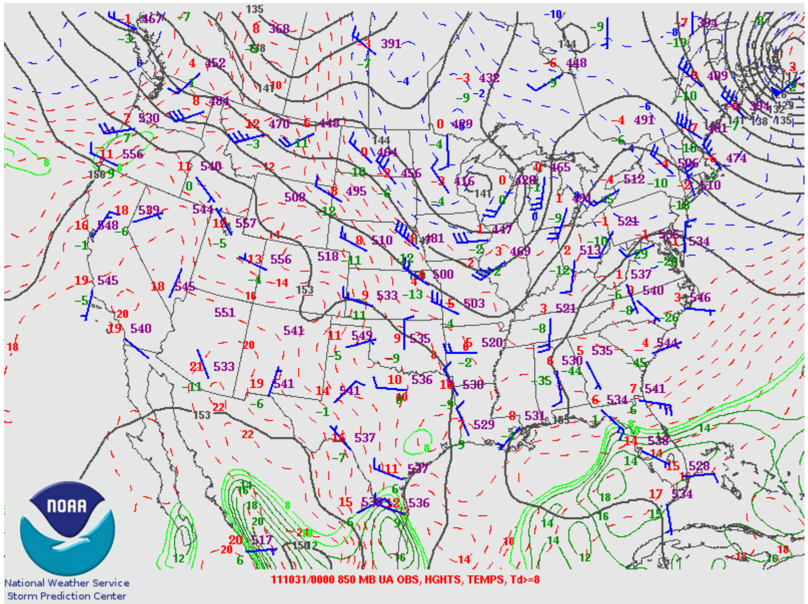

Figure 8. 850-mb observations and objectively-analyzed 850-mb heights (black), isotherms (dashed red and blue), isodrosotherms (green), and wind barbs (corresponding wind speeds in knots) at 0000 UTC 31 October 2011.

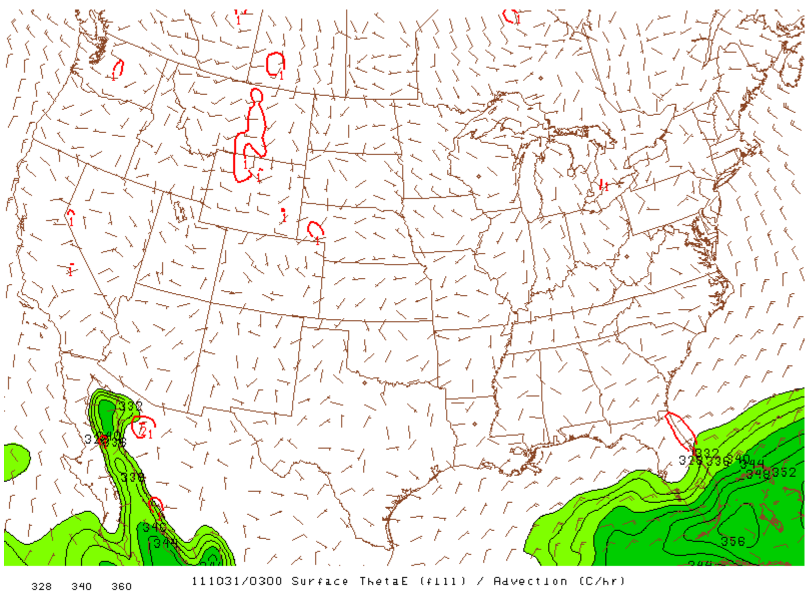

Figure 9. RUC-2 analysis output (using 40-km grid spacing), including surface theta-e (in green color fill and in units of kelvins), wind barbs (corresponding wind speeds in knots), and surface thermal advection (in red contours).

d. *Storm motion*

While the ingredients for deep, moist convection producing heavy rainfall during this event are well established through inspection of the 0000 UTC Miami RAOB, synoptic weather maps, and other observations, we still have not addressed why a stationary supercell ensued. To further investigate this aspect of the heavy rain event, we explore the vertical wind profile (Fig.

5) and corresponding hodograph (Fig. 10). Weak to moderate east-northeasterly flow in the low levels quickly veered to south-southwesterly above 850 mb, with the winds gradually veering and increasing in strength into the mid and upper levels. Despite the presence of modest mid-level flow (around 20 knots at 500 mb), the easterly and northerly low-level winds reduced the cloud-bearing mean flow by opposing the mid-level southwesterlies.

The wind profile, especially with its vertically varying direction (nearly 180° from the surface to 500 mb), supported at least some threat for supercells, with an effective bulk shear magnitude (Thompson et al. 2007) of 39 knots. The storm did develop persistent mid-level mesocyclones. A radar sequence through most of the event, which includes illustration of the mid-level mesocyclone, is presented in Fig. 11 (animation). [Note: Key West Weather Surveillance Radar (WSR)-88D data are presented, as the Miami WSR-88D data were not available during this event]. The presence of such persistent mesoscyclones represents a vertical perturbation pressure gradient which enhances vertical motion and/or ascent at the storm scale.

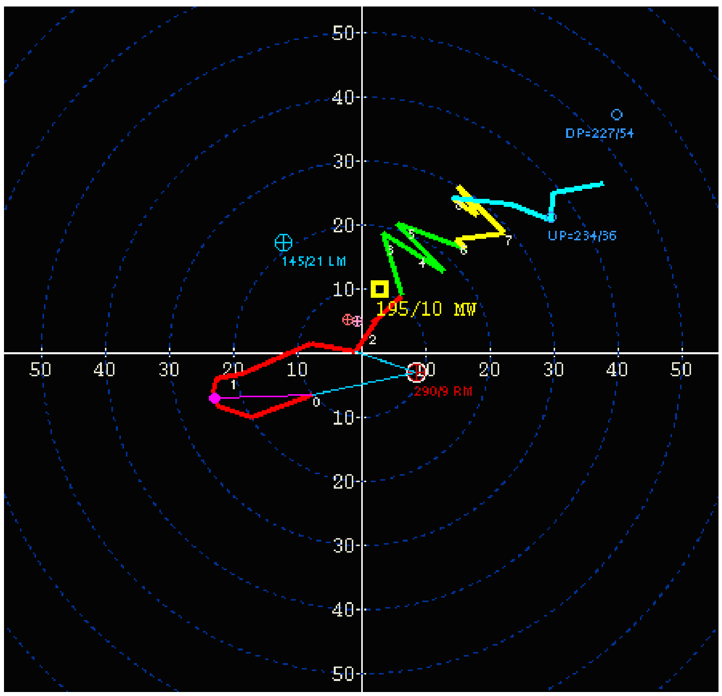

Figure 10. Observed hodograph data at Miami, 0000 UTC 31 October 2011. Hodograph curve is color-coded by height above ground (red generally corresponds to the lowest 3 km, green generally corresponds to the 3–6-km layer, yellow generally corresponds to the 6–9-km layer, and blue generally corresponds to the layer above the 9-km level), with small white numbers beside the line indicating height in km at corresponding points along the curve. Supercell motions for a theoretical right-moving (RM) supercell and a theoretical left-moving (LM) derived supercell (Bunkers et al. 2000) are plotted. The "RM" corresponds to a right-moving supercell moving east-southeastward at 9 knots and the "LM" corresponds to a left-moving supercell moving northwestward at 21 knots.

Applying the Bunkers et al. (2000) supercell motion technique to the 0000 UTC Miami data, a right-moving supercell would be expected to move from the west-northwest (290°) at 9 knots. However, what was observed was negligible mean storm motion. This is not surprising, because (1) small variations in the vertical wind profile would reduce storm motion for a right-moving supercell. For example, a slight veering of the 0–0.5-km flow, such that it attains more of an easterly component and less of a northerly component, would yield some veering of the 0–0.5 to 5.5–6-km bulk vertical wind shear vector. This would displace the tip of the storm-motion vector closer to the origin of the hodograph (i.e., representing zero storm motion). Modifications to the background near-storm environment resulting from hydrodynamic pressure perturbations in association with the supercell also could have modified the wind profile and induced changes in the background low-level flow. And (2) the mean absolute error for the Bunkers et al. (2000) technique was reported to be around 4 m s^{-1} (7.8 knots). Factoring this potential error into the estimated motion for a right-moving supercell, a near-zero storm motion for a developed supercell may be considered within the realm of possibilities for storm motion in this case.

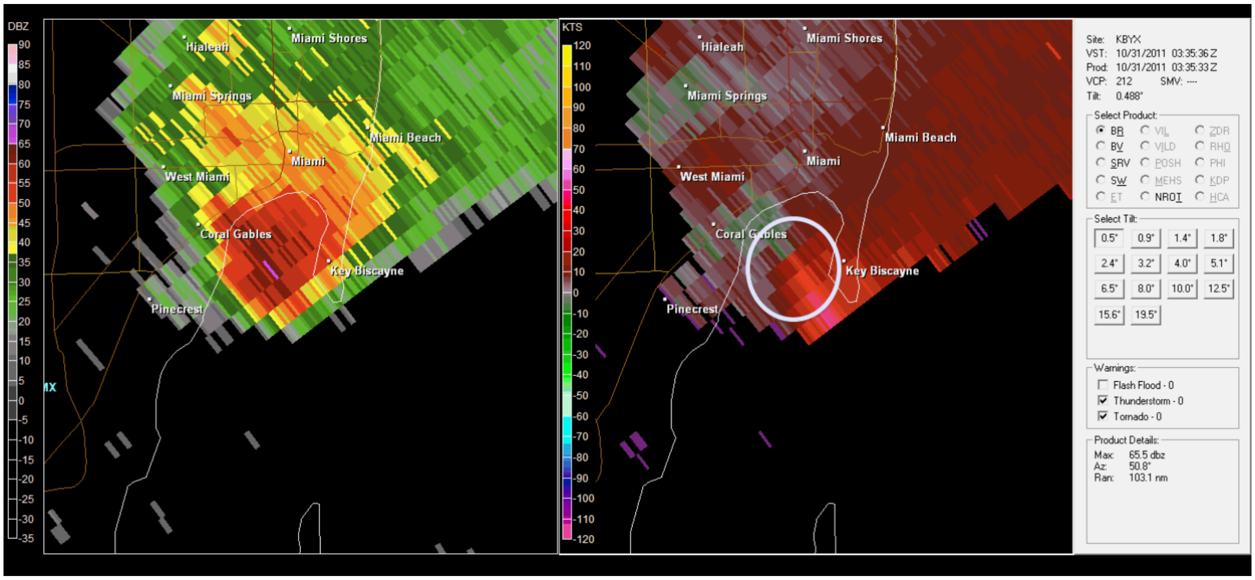

Figure 11. Radar animation (from Key West, Florida WSR-88D, located about 200 km southwest of Miami), 0000 UTC to 0700 UTC 31 October 2011. Left panel depicts 0.5-degree reflectivity [around 3962 m (13000 ft.) above ground level] and right panel storm-relative velocity. Ellipses are placed in the right panel to highlight the approximate location of any identifiable mesocyclone. **(Please click on the above image for an animation.)**

In addition to clues from the vertical wind profile that near-zero storm motion was supported, thermodynamic considerations also are consistent with the observed nearly stationary nature of the convection. The 0000 UTC Miami sounding (Fig. 5) reveals the absence of appreciable dry layers, and the presence of a nearly saturated adiabatic thermal profile in the lower and middle levels. This profile, featuring weak low-to-mid-level lapse rates, minimizes the strength of storm-induced cold pools, owing, in part, to the lack of evaporational cooling in convective downdrafts (James and Markowski 2010). Propagation away from the center of the supercell storm likely was minimized, further limiting net storm motion.

Considering the relatively low-end magnitude of deep shear for supercell storms, it is not surprising that the animation (Fig. 11) suggested the storm occasionally exhibiting multicellular characteristics (e.g., instances of flanking convection merging with the primary storm cell). Convective propagation associated a multicellular mode may have modulated storm motion, in addition to processes inherent to the supercell structure. Such propagation may have been supported by the interaction of the low-level flow regime with the presumably weak cold pool associated with the convection. Furthermore, propagation may also have been supported by coastal/mesoscale effects that may have played a secondary role in anchoring the supercell to the coast. This will be discussed in greater detail within the following section. However, the aforementioned primary arguments are directly evident in observational and sounding data which put in the context of the existing synoptic and mesoscale environments can greatly aid in identifying the threat for heavy rainfall and flash flooding leading up to the event and during the storm lifecycle too.

e. *Coastal effects*

To better understand the role that coastal effects may have played in modulating the near-storm environment such that convection remained stationary, the third version of the Advanced Weather Research and Forecasting (WRF) model (e.g., Skamarock et al. 2008; WRF Users Page 2012) was used in simulating the environment. A nest featuring 0.5-km horizontal grid spacing encompassing the Miami area was embedded within a parent domain of 1.5-km grid spacing covering a larger part of southeastern Florida (Fig. 12). Such small grid spacing was used to more accurately represent micro-scale coastal effects.

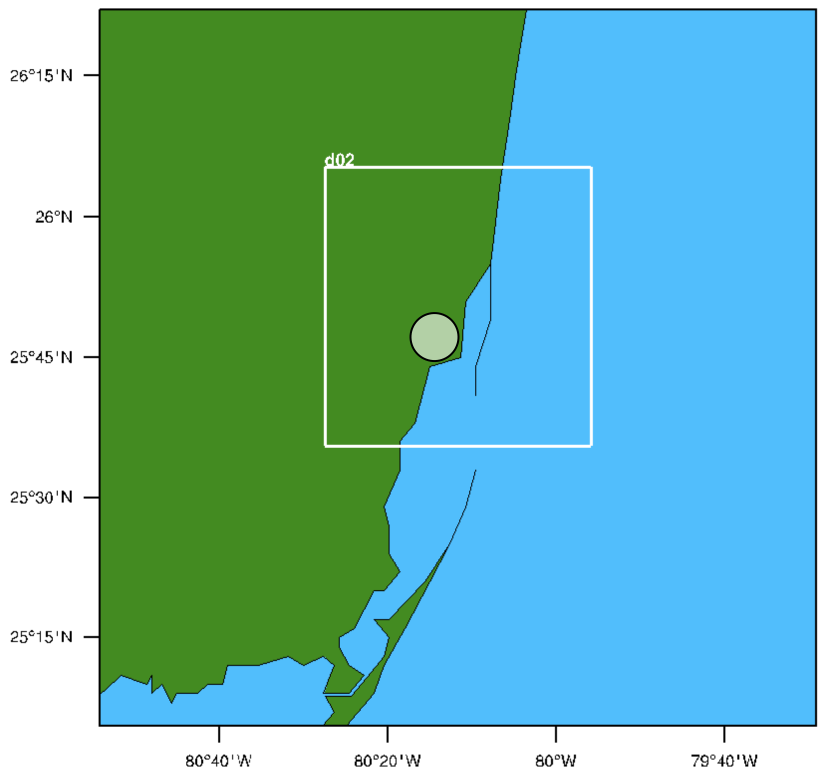

Figure 12. WRF domain configuration for the 30-31 October 2011 simulation. Inner domain applies 0.5-km grid spacing, whereas outer domain applies 1.5-km grid spacing. The white, semi-transparent ellipse indicates the approximate position of Miami for simple geographical reference.

Boundary conditions were provided by the NCEP FNL (Final) Operational Global Analysis (Computational and Information Systems Laboratory at the National Center for Atmospheric Research 2012) output on a 1.0° x 1.0° mesh. Despite the coarse mesh of the FNL output relative to the nested domains, we speculate that the downscaling process invoked in running the WRF simulation would still yield valuable information in a diagnostic mode for evaluating physical processes at play during the heavy rainfall event. This is because the large-scale pattern is captured within the coarser-resolution boundary conditions and is partly what drives the mesoscale and smaller-scale patterns supporting the heavy rain event. The coarser-resolution boundary conditions are also more representative of the limited spatiotemporal sampling of the atmosphere through the current observing network. As will be revealed within the present study, such a method is practical, as the WRF output results appeared sound and processes in the WRF simulation are able to account for the downscaling process.

Computations are performed over 28 vertical levels using a time-step of 3 seconds. The microphysics package involved the WRF single-moment 3-class scheme (Hong et al. 2004). For the lower levels, the Yonsei University scheme (Hong et al. 2006) was used as the planetary boundary layer scheme, while the Noah Land Surface Model (Ek et al. 2003) was also used. Other parameterization schemes or ensembles of parameterization or physics schemes could have been used, but were not, because of 1) limited computational resources available and 2) focusing on the effect of using different boundary layer and or physics schemes (or finding an ideal way of standardizing a simulation relevant for exploring the potential for flash flooding from a modeling perspective) was beyond the scope of this short paper. Two simulations for this event were run: one using initial conditions at 0000 UTC 31 October and the other using initial conditions at 1200 UTC 30 October. While these simulations did not appear to provide an accurate representation of the observed convective evolution based on simulated reflectivity and precipitation output (not shown), they are not intended to exactly replicate the event (especially with regard to the evolution of convection). Rather, it is intended that the simulations represent the background thermodynamic and kinematic environment supporting convection in the real atmosphere. Such simulation results may prove useful in illustrating background mass fields perhaps supporting convection especially at the storm scale leading up to the event. They may also provide local modelers with considerations for addressing the problem of forecasting flash floods based on the utility of high-resolution WRF output.

1) 0000 UTC 31 October simulation

Selected output for this simulation using 0000 UTC 31 October 2011 initial conditions is presented in Fig. 13. Relatively cooler temperatures resulting from diabatic effects from nocturnal cooling over land areas supported the coastal gradient in the theta-e that lies along the coast. While such a scenario would otherwise support the development of an eastward-propagating land-breeze boundary off the southeast Florida coast, the background easterly flow component provides a land-ward, advective component to the land-breeze circulation that counters its ocean-ward propagation, maintaining the nearly stationary coastal convergence zone along the coast. Ascent associated with the solenoidal circulation attendant to the coastal baroclinic zone would have been augmented by the ascending branch of the land breeze circulation if the two exhibited spatial alignment. Note the apparent theta-e deficit event east of Biscayne Bay. This feature is a model artifact, as it represents surface diabatic cooling process over the model's representation of Key Biscayne. In reality, such a theta-e gradient would likely be very different in spatial distribution and magnitude from that represented in this model simulation. This deficit appeared to have a very localized spatial influence on the simulation results, as neither its shape nor its orientation exhibits any appreciable variation throughout the duration of the simulation with very similar quantities of meteorological parameters found both upstream and downstream of the deficit (Fig. 13). As such, it likely posed no importance for the understanding of the mesoscale or storm-scale environment supporting the heavy rain event.

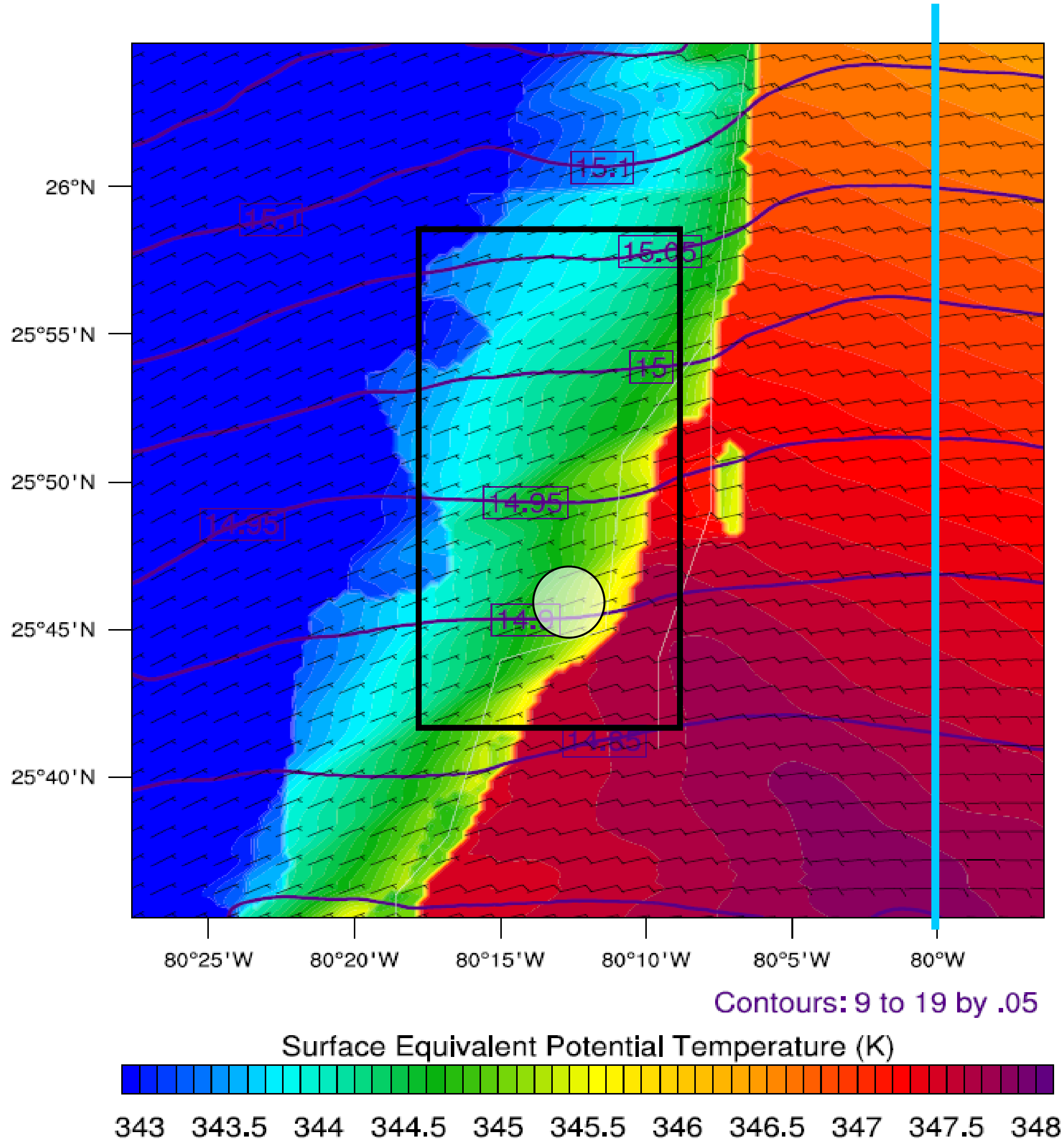

Figure 13. Mean sea level pressure departure from 1000 mb (purple contours), theta-e (in color fill, K), and wind barbs (corresponding wind speeds in knots) from the 0000 UTC WRF simulation computed at 0300 UTC 31 October 2011. Geographical boundaries are roughly depicted by thin white lines west of 80°W longitude (marked by relatively bolder light blue line). Rectangle with solid black outline approximately represents the areas depicted in Fig. 14. The white, semi-transparent ellipse indicates the approximate position of Miami for simple geographical reference.

The role of surface roughness and friction is well evident in the surface wind field, as wind speeds over land are less than those over water, resulting in a band of frictionally-induced, low-level convergence oriented along the coast in the vicinity of the coastal baroclinic zone (Fig.

14). Note that the 40-m divergence (negative convergence) is investigated in this simulation, as it may provide some semblance of the convergence present within the boundary layer just above the surface (implying some depth to the convergence). The low-level convergence and implied ascent are likely associated with a mostly east-northeasterly to easterly surface flow regime that increases immediately east of the coastline.

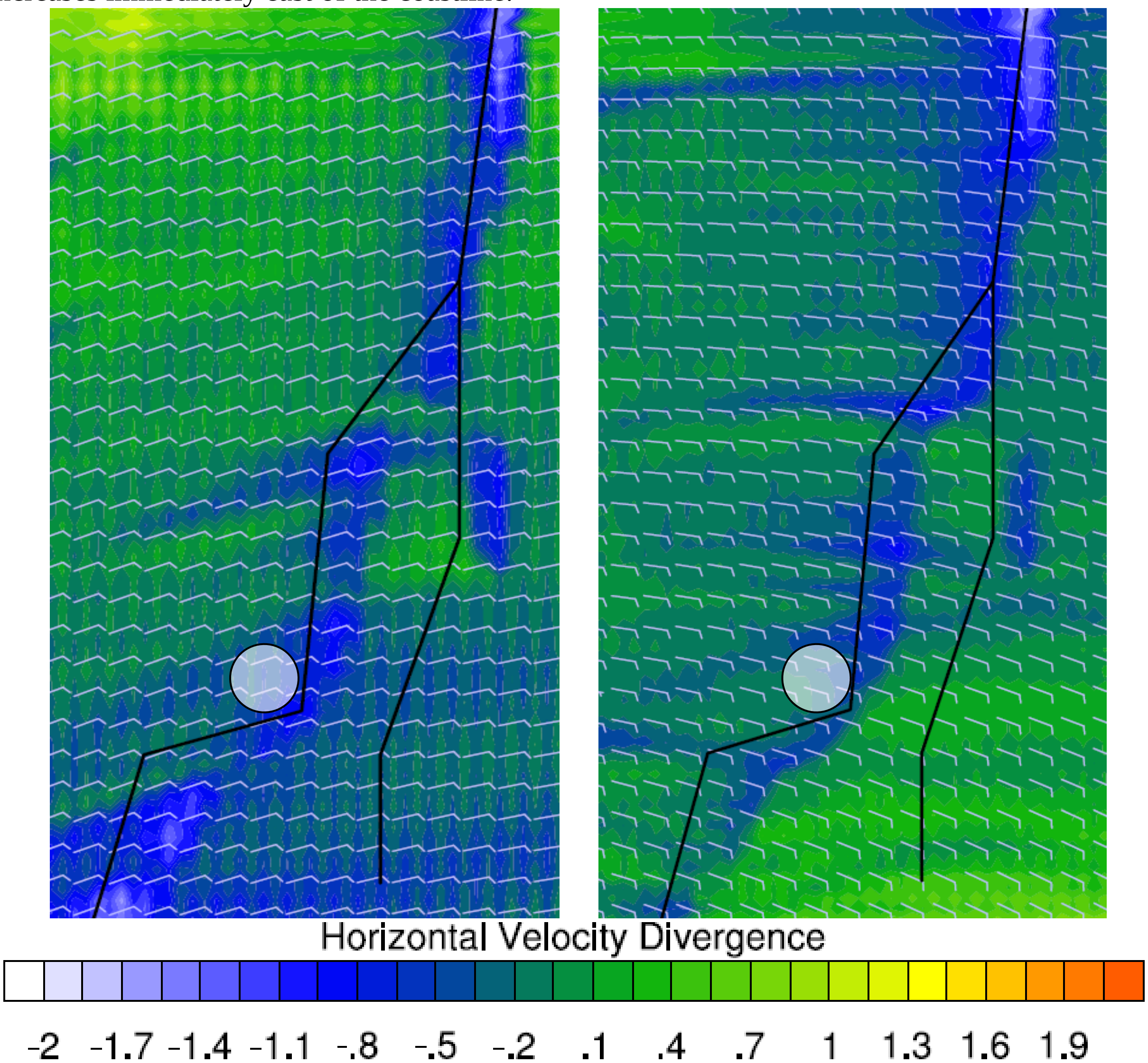

Figure 14. Horizontal velocity divergence (μs^{-1}, in color fill) and wind barbs (kt) at 40 m above mean sea level from the 0000 UTC WRF simulation computed at 0300 UTC (left) and 0600 UTC (right) 31 October 2011. Geographical boundaries are roughly depicted by black lines. The area depicted corresponds to the region indicated by the rectangle with the solid black outline in Fig. 13. The white, semi-transparent ellipse indicates the approximate position of Miami for simple geographical reference.

It follows that localized coastal effects may have provided additional support for stationary convection, evidenced by the mostly terrain-anchored nature of the low-level convergence. Terrain-induced effects may have played a role in anchoring the convection, and local WRF simulations could provide some insight into their existence and magnitude as shown in this case. Given the background kinematic and thermodynamic conditions favoring stationary convection, at the very least it appears that terrain effects certainly did not reduce chances for stationary convection.

2) 1200 UTC 30 October simulation

A separate model simulation for the daytime prior to the flash flood event was run using initial conditions from 1200 UTC 30 October 2011. The across-coast wind speed differences and the strength of the persistent, organized low-level convergence features are relatively less than those quantities during the post-dusk hours (not shown), likely reflecting the result of downward transport of higher momentum over land areas in association with boundary layer circulations. These circulations are reflected by the noisiness of the theta-e field over land. Accordingly, nocturnal cooling may have provided some influence in strengthening low-level convergence and maintenance of convection.

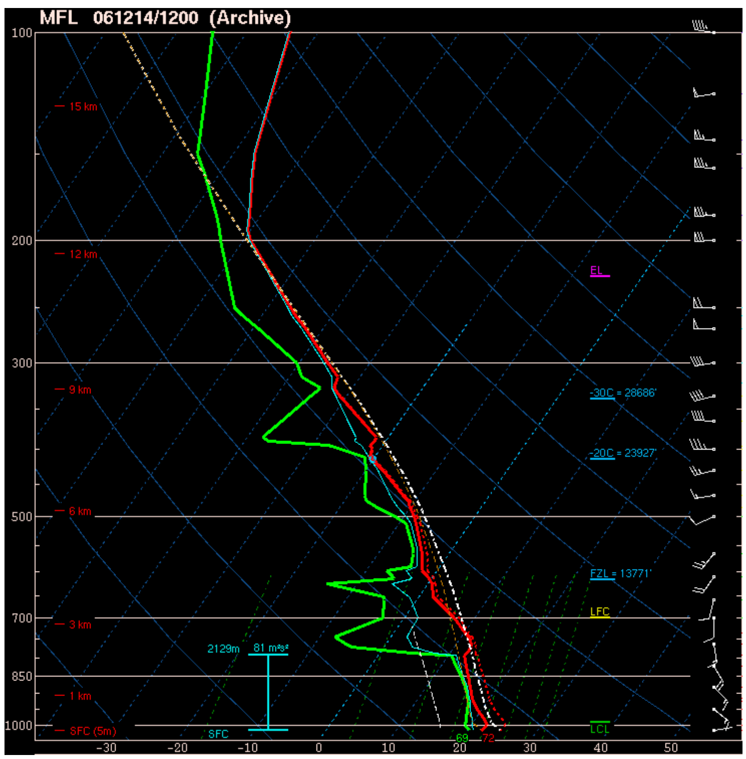

Figure 15. Observed sounding data at 1200 UTC 14 December 2006 from Miami, FL. The sounding depiction follows the same convection as in Fig. 5.

3. Other flash flooding events

Other noteworthy flash flood events, with similar evolutions to the 30–31 October 2011 case, took place over portions of south Florida on 14 December 2006 (Strassberg 2009) and 17 December 2009. Corresponding RAOB data from Miami, FL are provided in Fig. 15 and Fig. 16. Substantial similarities exist between these soundings and that corresponding to the 30–31 October 2011 event (Fig. 5). However, the earlier events include the presence of relatively drier mid-level air and thus lower PWAT values [around 43.2 to 45.7 mm (1.7 to 1.8 in.)], although these differences are not negligible, they still highlight anomalously moist tropospheric conditions still present (Bunkers 2006). Many of the thermodynamic characteristics of these soundings, including the warm-cloud layer depths, low LCL heights, and "narrow"-CAPE profiles promote efficient precipitation processes. Furthermore, substantial similarities exist in the observed wind profiles between these two cases, supporting little, if any, storm motion. Using the Bunkers technique (Bunkers et al. 2000), right-moving supercell motions were anticipated to be around 10 knots, similar to the 30–31 December 2011 event, with motion potentially suppressed by factors discussed earlier with that case.

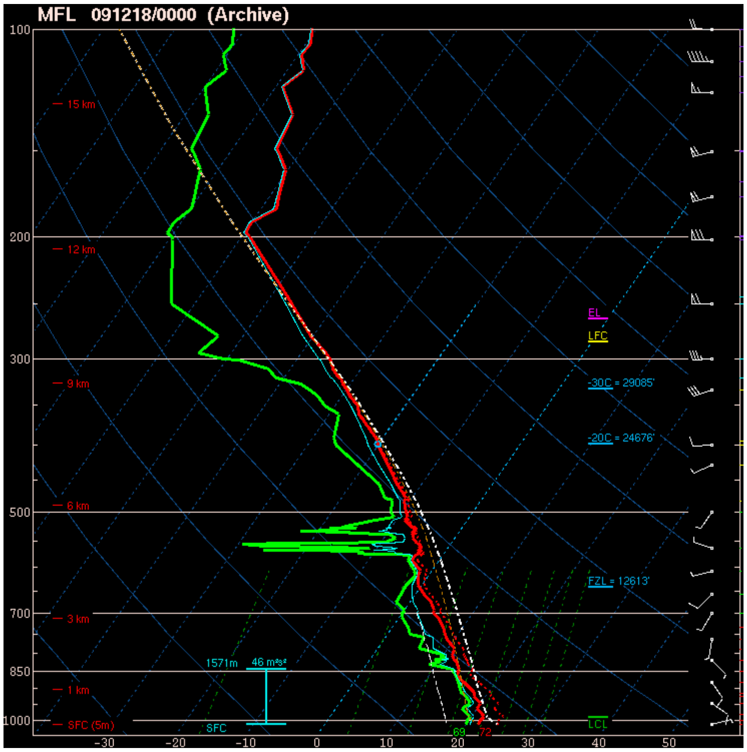

Figure 16. Observed sounding data at 1200 UTC 17 December 2009 from Miami, FL. The sounding depiction follows the same convection as in Fig. 5.

As with the 30–31 October 2011 case, the background environment for these cases featured a low-level baroclinic zone draped across parts of south Florida. Coastal convergence, the baroclinic circulation, and local mesoscale enhancements to low-level convergence favored low-level ascent. WRF simulations were run to identify some of the mesoscale processes based on a configuration identical to that for the 30–31 October 2011 (Fig. 17 and Fig. 18). While along-coast wind speed variations appeared larger in the 2009 case than in the 2006 case, and the surface winds were at an oblique angle to the coast for the 2006 case, both events were associated with a coastal baroclinic zone. Localized enhancements to the flow in association with the shape of the coastline and its modulation of the surface pressure pattern may have contributed to enhanced convergence along the coast. Simulated reflectivity and precipitation output indicate limited resemblance to observed data (not shown), though simulated mass fields may provide some support for perhaps anticipating the threat for convection as with the 30–31 October 2011 case particularly when put in the context of the preexisting synoptic, mesoscale, and thermodynamic environments.

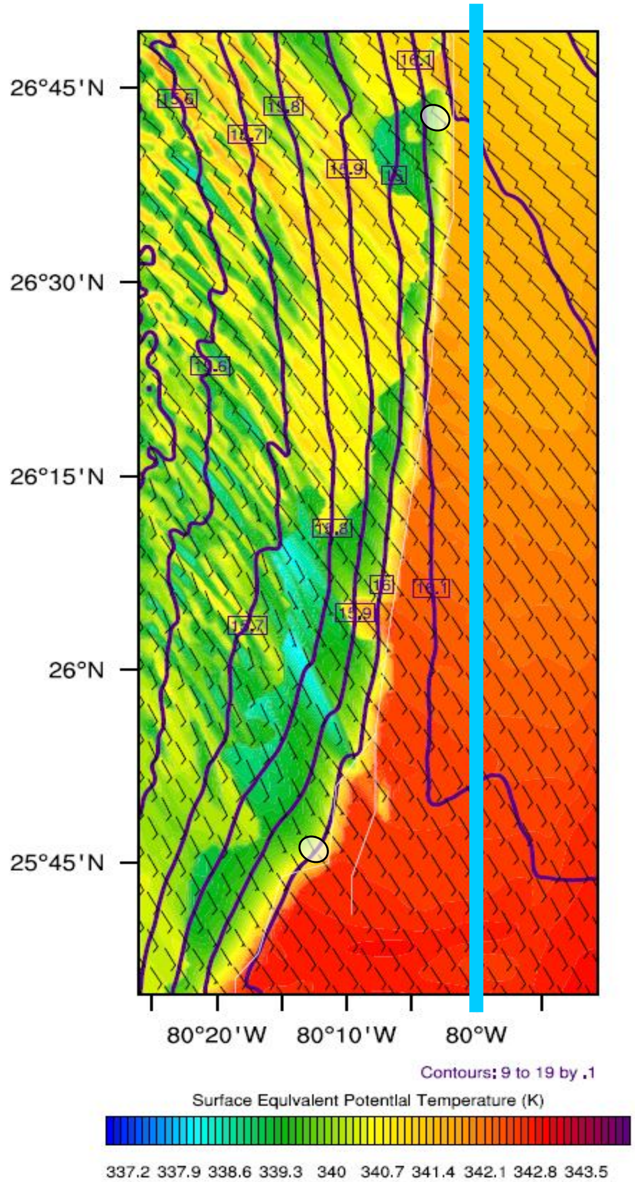

Figure 17. Mean sea level pressure departure from 1000 mb (purple contours), theta-e (in color fill, K), and wind barbs (corresponding wind speeds in knots) from the 1200 UTC on 14 December 2006 WRF simulation computed at 1800 UTC 14 December 2006. Geographical boundaries are roughly depicted by thin white lines west of 80°W longitude (marked by relatively bolder light blue line). Note the coastal baroclinic zone and coastal wind speed variations. The northern, white, semi-transparent ellipse indicates the approximate position of West Palm Beach; the southern, white, semi-transparent ellipse indicates the approximate position of Miami.

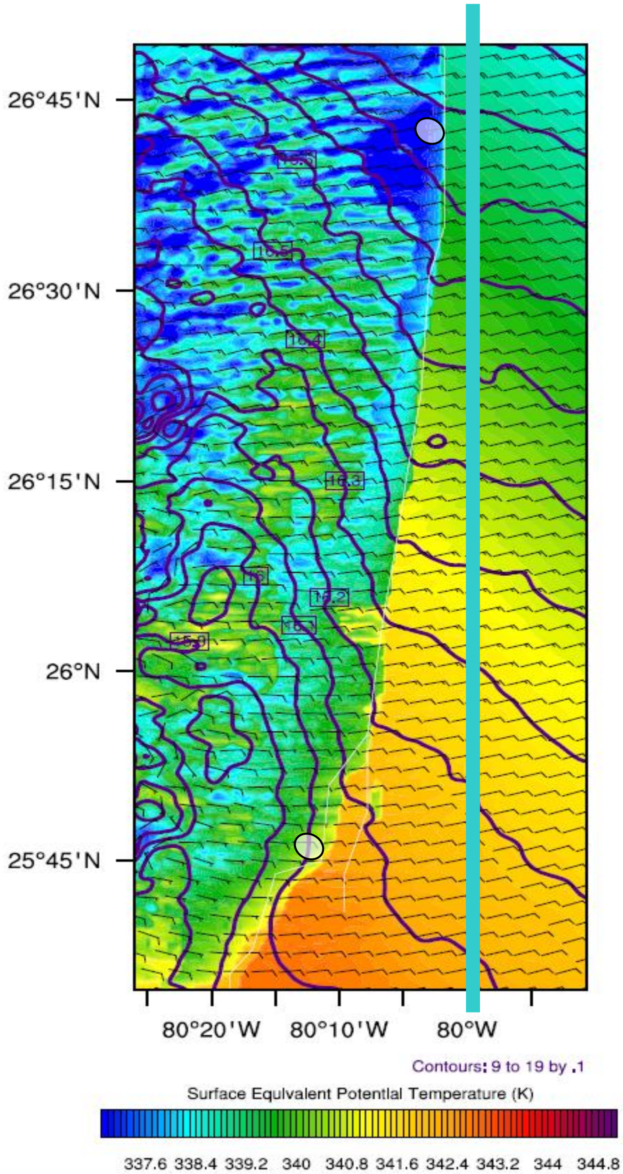

Figure 18. Mean sea level pressure departure from 1000 mb (purple contours), theta-e (in color fill, K), and wind barbs (corresponding wind speeds in knots) from the 1200 UTC on 17 December 2009 WRF simulation computed at 1800 UTC 17 December 2009. Geographical boundaries are roughly depicted by thin white lines west of 80°W longitude (marked by relatively bolder light blue line). Note the coastal baroclinic zone and coastal wind speed variations. The northern, white, semi-transparent ellipse indicates the approximate position of West Palm Beach; the southern, white, semi-transparent ellipse indicates the approximate position of Miami.

4. Conclusions

Supercell thunderstorm activity was responsible for producing excessive rainfall across parts of the Miami area during a several-hour period on 30 and 31 October 2011. The rain produced by this nearly stationary storm produced flash flooding along with substantial costs to residences and businesses. This paper identifies key clues evident in observational and high resolution modeling data that would suggest the potential for flash flooding, especially when combined with antecedent rainfall.

Based on sounding data, rich tropospheric moisture content, the presence of a low-level front, and coastal convergence are all characteristic of this environment. Furthermore, ingredients enhancing precipitation efficiency were investigated for the 30–31 October 2011 case which revealed a "narrow"-CAPE layer, low LCL height, and deep warm-cloud layer. Applying the Bunkers supercell technique, near-zero storm motion was established to be within the range of possibilities for a right-moving supercell motion given the observed wind profile. The potential for negligible storm motion may be assessed using the Bunkers et al. (2000) supercell motion technique, after having identified an environment that supports supercells. Upon initiation of a supercell, forecasters may consider paying special attention to its initial characteristics and motion based on radar data, as a slow-moving or nearly stationary supercell may persist depending on environmental characteristics. Mesoscale effects may also have played a role in locally enhancing forced ascent via low-level convergence per WRF simulations that addressed mesoscale forcing for ascent in association with terrain. These mesoscale effects may have provided additional support for anchoring convection given the background kinematic and thermodynamic environment. Similar observations were noted for two other cases discussed in this paper.

While no simple parameter or guideline may be used to consistently forecast heavy rainfall and flash flooding with accuracy, we have identified some key ingredients that came together to support substantial heavy rain events over south Florida in a few cases. The analysis of observational data was found to be fundamental in identifying these ingredients and anticipating the threat, and high-resolution model output may also aid in the identification process. While some degree of uncertainty is inherent to any forecast process, sufficient evidence was present to anticipate heavy rainfall and flash flooding given a right-moving supercell during the 30–31 October 2011 event, especially given the availability of Miami RAOB data and others surrounding data networks such as GPSMET. Identification of similar environments may alert forecasters to the threat for flash flooding while considering local terrain effects that could exacerbate this threat.

Finally, this study did not address null cases where these ingredients were present and no flash flooding resulted. The authors believe that is a key ingredient for a more comprehensive approach to this problem but is beyond the scope of this short paper. The main aim here was to identify ingredients leading to the recognition of an increased threat or potential for flash flooding resulting in increased situational awareness in the forecast and warning process.

Acknowledgements. The authors are grateful for the thorough review of this work by Mr. Stephen Corfidi of the Storm Prediction Center (SPC), as well as the initial motivation from Mr. John Hart of the SPC to explore the forecast problem of south Florida coastal convection in detail. Dr. Larry Carey and an anonymous reviewer provided helpful feedback in improving the quality of this work. Mr. Richard Thompson of the SPC offered beneficial guidance in orchestrating an appropriate procedure for analyzing this problem, especially with regard to its observational focus. Output displays for sounding data and hodograph data are provided by National Centers Advanced Weather Interactive Processing System Skew T Hodograph Analysis and Research Program (NSHARP; Hart et al. 1999). Upper air analyses and RUC-2 analysis output are provided from links from the Storm Prediction Center (2012) website available at

http://www.spc.noaa.gov. Precipitation estimation is provided through the National Mosaic and Multi-Sensor QPE website available at http://nmq.ou.edu.

REFERENCES

Bunkers, M. J., cited 2006: Precipitable water plots: U.S. radiosonde locations for PW climatology. [Available online at http://www.crh.noaa.gov/unr/?n=pw.]

———, B. A. Klimowski, J. W. Zeitler, R. L. Thompson, M. L. Weisman, 2000: Predicting supercell motion using a new hodograph technique. *Wea. Forecasting*, **15**, 61–79.

Burpee, R. W., 1979: Peninsula-scale convergence in the south Florida sea breeze. *Mon. Wea. Rev.*, **107**, 852–860.

Caracena, F., R. A. Maddox, L. R. Hoxit, and C. F. Chappell, 1979: Mesoanalysis of the Big Thompson storm. *Mon. Wea. Rev.*, **107**, 1–17.

Chappell, C. F., 1986: Quasi-stationary convective events. *Mesoscale Meteorology and Forecasting*, P. S. Ray, Ed., Amer. Meteor. Soc., 289–310.

Computational and Information Systems Laboratory at the National Center for Atmospheric Research, cited 2012: NCEP FNL operational model global tropospheric analyses, continuing from July 1999. [Available online at http://dss.ucar.edu/datasets/ds083.2/.]

Doswell, C. A., III, and E. N. Rasmussen, 1994: The effect of neglecting the virtual temperature correction on CAPE calculations. *Wea. Forecasting*, **9**, 625-629.

———, H. Brooks, and R. Maddox, 1996: Flash flood forecasting: An ingredient-based methodology. *Wea. Forecasting*, **11**, 560–581.

Ek, M. B., K. E. Mitchell, Y. Lin, P. Grunmann, E. Rodgers, G. Gayno, and V. Koren, 2003: Implementation of the upgraded Noah land-surface model in the NCEP operational mesoscale Eta model. *J. Geophys. Res.*, **108**, 8851, doi:10.1029/ 2002JD003296.

Gutman, S. I., S. R. Sahm, S. G. Benjamin, B. E. Schwartz, K. L. Holub, J. Q. Stewart, and T. L. Smith, 2004: Rapid retrieval and assimilation of ground based GPS precipitable water observations at the NOAA Forecast Systems Laboratory: Impact on weather forecasts. *J. Meteor. Soc. Japan,* **82,** 351-360.

Hart, J. A., J. Whistler, R. Lindsay, and M. Kay, 1999: NSHARP, version 3.10. Storm Prediction Center, National Centers for Environmental Prediction, Norman, OK, 33 pp.

Hong, S. Y., J. Dudhia, and S. H. Chen, 2004: A revised approach to ice microphysical processes for the bulk parameterization of clouds and precipitation. *Mon. Wea. Rev.*, **132**, 103–120.

———, Y. Noh, and J. Dudhia, 2006: A new vertical diffusion package with an explicit treatment of entrainment processes. *Mon. Wea. Rev.*, **134**, 2318–2341.

James, R. P., and P. M. Markowski, 2010: A numerical investigation of the effects of dry air aloft on deep convection. *Mon. Wea. Rev.*, **138**, 140–161.

Maddox, R. A., L. R., Hoxit, C. F. Chappell, and F. Caracena, 1978: Comparison of meteorological aspects of the Big Thompson and Rapid City flash floods. *Mon. Wea. Rev.*, **106**, 375–389.

———, C. F. Chappell, and L. R. Hoxit, 1979: Synoptic and meso-α aspects of flash flood events. *Bull. Amer. Meteor. Soc.*, **60**, 115–123.

Petersen, W. A., L. D. Carey, S. A. Rutledge, J. C. Knievel, and R. H. Johnson, 1999: Mesoscale and radar observations of the Fort Collins flash flood of 28 July 1997. *Bull. Amer. Meteor. Soc.*, **80**, 191–216.

Skamarock, W. C., J. B. Klemp, J. Dudhia, D. O. Gill, D. M. Barker, M. G. Duda, X.-Y. Huang, W. Wang, and J. G. Powers, 2008: A description of the Advanced Research WRF version 3. NCAR Tech. Note TN-475+STR, 113 pp.

Strassberg, G., 2009: Mesoscale elements of the 14 December 2006 West Palm Beach flash flood. *Electronic J. Operational Meteor*., **10 (5)**, 1–28.

Thompson, R. L., C. M. Mead, R. Edwards, 2007: Effective storm-relative helicity and bulk shear in supercell thunderstorm environments. *Wea. Forecasting*, **22**, 102–115.

WRF Users Page cited, 2012: Chapter 5: WRF Model. [Available online: http://www.mmm.ucar.edu/wrf/users/docs/user_guide_V3/users_guide_chap5.htm.]